

4 Raman lidar remote sensing of geophysical media

Aleksey V. Malinka

4.1 Introduction

Lidars are equipment, consisting of a laser and a photo-receiver, that measures the backward scattering of light. They appeared in the 1960s (Fiocco and Smullin, 1963), i.e., immediately after the invention of the laser, and since then they have been actively used in the problems of natural media monitoring. Lidars are of great use in providing atmosphere and ocean pollution control, in control of atmospheric gases, and in measuring meteorological and climate characteristics. Generation of a beam of high power and small angular divergence makes the great advantage of lidars over projector sounding, having existed before. The possibility of accurate wavelength tuning, as well as spectral return measuring, allows the determination of the chemical composition of the atmosphere and the biochemical composition of the ocean. Thanks to the measurement of scattered light polarization degree one can learn about the shape of scatterers. Furthermore, as lasers are able to generate powerful pulses of short duration, there appears the possibility of measuring time-dependent returns, i.e., measuring not only the integral optical characteristics of a medium, but also their spatial distribution. These features made lidars a powerful tool in the investigation of geophysical media.

Besides the usual, elastic, lidar sounding, recently the methods of inelastic, particularly Raman, lidar sounding, have been developed. These methods provide a wide range of new possibilities (Ansmann et al., 1990, 1992a; Reichardt et al., 1996). Raman lidar sounding implies sounding based on receiving the signal of Raman scattering, in which the scattered light shifts frequency to a value equal to the eigenfrequency of a molecule of the scattering substance. The Raman lidar return is proportional to the scattering substance concentration. Thus, measuring the Raman lidar return allows one to establish the presence of substances whose eigenfrequencies correspond to lines in the measured spectrum. On the other hand, well-known characteristics of Raman scattering by stable components (nitrogen in the atmosphere and water in the ocean) permits the use of the Raman lidar return as a reference (calibration) signal for other measurements.

The growing interest in Raman sounding methods is not only due to their advantages and their additional possibilities. It is also due to the fact that the technical capabilities to fix the weak light signal have been steadily improving. For example, thirty years ago Raman scattering by atmospheric nitrogen in a pulse lidar regime could be fixed from altitudes of up to 3 km (Cohen et al., 1978). Nowadays the Raman lidar return is accurately fixed from altitudes of 30 km and more (Ansmann et al., 1992b; Sherlock et al., 1999a). Even the possibility of spaceborne Raman lidar measurement is discussed (Girolamo et al., 2006).

Joint use of both elastic and inelastic, including Raman, scattering suggests a future trend to discover new ways of sounding and measuring properties of various turbid media.

Nowadays, most of the methods of medium characteristics retrieval use the lidar equation within the framework of single scattering approximation. They consider multiple scattering as an interference to be suppressed. However, as many authors have mentioned, in most geophysical media (such as clouds, dense aerosols or seawater) multiple scattering plays the key role in lidar return forming (Bruscaglioni et al., 1999; Eloranta, 1972; Reichardt et al., 2000; Weinman and Shipley, 1972). There are also lidar systems, in which the signal is completely defined by multiple scattering. These are multiple-field-of-view lidars (that measure light fluxes at several angle intervals) (Bissonnette and Hutt, 1990; Roy et al., 1997) and imaging lidars (that measure the irradiance distribution in the focal plane of the receiver, i.e., the angular distribution of radiance at the entrance of the receiver optics) (Muscari et al., 1996). In both cases, the problem is not to estimate the contribution of multiple scattering as some correction, but to describe it correctly in a qualitative and quantitative way.

The problem of multiple scattering in lidar measurements is a focus of interest of the international workshop MUSCLE (MUltiple SCattering in Lidar Experiments), which has succeeded both in simulation of multiple scattering and in its use in the inverse problem s for the case of elastic lidar sounding (Muscari et al., 1996; Zege et al., 2003a; Bruscaglioni et al., 1999). However, for a long time few attempts were made to simulate multiple scattering for Raman lidar sounding (Bruscaglioni et al., 1999; Wandinger, 1998) and practically no attempts were made to include it in the inverse problem.

This chapter gives a short review of the existing methods of Raman lidar sounding of geophysical media, and it presents the theory for the Raman lidar return with multiple scattering and the new methods of using multiple scattering to retrieve the microphysical characteristics of a light scattering medium.

4.2 Review of the existing methods of Raman lidar sounding

The idea of using Raman scattering in lidar sounding of geophysical media appeared in the 1960s. However its implementation was delayed, primarily because of the weak signal power. In the late 1970s, there appeared lidar measurements of Raman scattering from water while sounding ocean (Klyshko and Fadeev,

1978). Methods of fixing Raman scattering from atmospheric nitrogen were suggested by Egert et al. (1983). Nowadays there are a lot of lidar systems all over the world. These systems make it possible to measure Raman scattering not only from atmospheric nitrogen, but also from water vapour and other atmospheric gases of low concentration, not to mention seawater. Raman lidar is a common instrument to get information about the composition of the sounding medium, its temperature and humidity (for atmosphere), and about the presence of suspended particles (cloud droplets, aerosols, hydrosols), their chemical properties and sizes (Ansmann et al., 1990, 1992a, 1992b; Reichardt et al., 1996, 2000; Wandinger et al., 1995; Roy et al., 1997; Sherlock et al., 1999a, 1999b; Whiteman and Melfi, 1999).

This chapter describes the main modern methods of sounding and processing the Raman lidar return.

4.2.1 Lidar equation

The lidar equation is an expression that relates the lidar return $F(z)$ (the energy of light coming from the depth interval from z to $z + dz$ divided by dz) to optical medium characteristics and lidar system parameters. Usually it is written in the framework of the single scattering approximation. For elastic lidar return it has the form:

$$F(z) = A\sigma(z, \pi) \exp\left(-2 \int_0^z \varepsilon(z') dz'\right), \quad (4.1)$$

where A is a calibration constant, including energetic characteristics of the lidar system, geometric parameters of the experiment and refractive index of sounding medium, $\sigma(z, \pi)$ is the backscattering coefficient, $\varepsilon(z)$ is the extinction coefficient, and z is the sounding depth.

The time t the photon arrives at the receiver is related to the depth z the photon penetrates into the medium by the following expression:

$$t = 2 \frac{H + z}{c}, \quad (4.2)$$

where H is the distance from the lidar to the nearest medium border, c is the speed of light in air.

The expression for the Raman lidar return in the framework of the single scattering approximation is:

$$F_R(z) = A\sigma_R(z, \pi) \exp\left(-\int_0^z [\varepsilon(z', \lambda_0) + \varepsilon(z', \lambda_R)] dz'\right), \quad (4.3)$$

where $\sigma_R(z, \pi)$ is the Raman backscattering coefficient, λ_0 is the initial wavelength, and λ_R is the Raman shifted wavelength, the initial and shifted wavelengths being related as:

$$\lambda_R = \frac{1}{1/\lambda_0 - \delta\tilde{\nu}}, \quad (4.4)$$

where $\delta\nu$ is a Raman frequency shift, depending on an eigenfrequency of a molecule.

Unlike high-spectral-resolution lidars (Grund and Eloranta, 1991; Shipley et al., 1983; Piironen and Eloranta, 1994), Raman lidars have a receiver frequency band broader than the width of the appropriate Raman line, so all the light that is Raman scattered at the wavelength λ_0 is assumed to shift to the wavelength λ_R .

Equation (4.3) is the basic equation used to process Raman sounding data. The Raman backscattering coefficient $\sigma_R(z, \pi)$ is proportional to the concentration of scattering molecules. Therefore, the Raman lidar return is also proportional to the concentration of molecules, and so measuring the power of the Raman lidar return enables the estimation of the concentrations. However, such a straight way is not a very accurate one, because the extinction coefficient remains unknown. For real measurements, other methods are applied. They are discussed below.

4.2.2 The method of Raman reference signal

The idea of the method is to measure two different Raman signals simultaneously. In this case, one signal is used to measure concentration, and the other is used as a reference signal (Ansmann et al., 1992a).

Let a laser pulse propagate into the atmosphere at the wavelength λ_0 and let the receiver fix two Raman scattering signals, one, for example, from atmospheric nitrogen and the other from water vapour. The powers of these lidar returns are

$$F_{H_2O} = A\sigma_R^{H_2O}(z, \pi) \exp\left(-\int_0^z [\varepsilon(z', \lambda_0) + \varepsilon(z', \lambda_{H_2O})] dz'\right), \quad (4.5)$$

$$F_{N_2} = A\sigma_R^{N_2}(z, \pi) \exp\left(-\int_0^z [\varepsilon(z', \lambda_0) + \varepsilon(z', \lambda_{N_2})] dz'\right). \quad (4.6)$$

Assuming that wavelengths λ_{H_2O} and λ_{N_2} differ slightly, i.e., the difference of the extinction coefficients at these wavelengths is negligible: $\varepsilon(z, \lambda_{H_2O}) \approx \varepsilon(z, \lambda_{N_2})$, we get for the ratio of these returns:

$$\frac{F_{H_2O}}{F_{N_2}} = \frac{\sigma_R^{H_2O}(z, \pi)}{\sigma_R^{N_2}(z, \pi)}. \quad (4.7)$$

The Raman backscattering coefficient is equal to the product of the Raman backscattering cross-section $Q(\pi)$ of one molecule by the concentration of molecules $n(z)$:

$$\sigma_R(z, \pi) = n(z)Q(\pi). \quad (4.8)$$

So, we get:

$$\frac{F_{H_2O}}{F_{N_2}} = \frac{Q^{H_2O}(\pi) n^{H_2O}(z)}{Q^{N_2}(\pi) n^{N_2}(z)}. \quad (4.9)$$

Whereas the nitrogen concentration is a stable quantity, in fact, Eq. (4.9) gives a straightforward way to measure the water vapour concentration profile (mixing

ratio). The humidity profile could be derived using the well-known formulas if an additional measurement of a temperature profile is carried out (Mattis et al., 2002).

4.2.3 The method of measuring an aerosol extinction profile with a Raman lidar

Raman scattering by nitrogen is also applied to investigation of aerosols (Ansmann et al., 1990; Reichardt et al., 1996). In this case, the power of the Raman lidar return can be written as:

$$F_R(z) = A \sigma_R^{N_2}(z, \pi) \exp\left(-\int_0^z [\varepsilon(z', \lambda_0) + \varepsilon(z', \lambda_R)] dz'\right), \quad (4.10)$$

backscattering being due to nitrogen (with a wavelength shift) and extinction being due to aerosol. If spectral difference of aerosol properties at λ_0 and λ_R is negligible (it is so, if sounding wavelengths do not match the absorption lines of aerosols or atmospheric gases), then we get:

$$\varepsilon(z) = -\frac{1}{2} \frac{d}{dz} \ln\left(\frac{F(z)}{A \sigma_R^{N_2}(z, \pi)}\right), \quad (4.11)$$

where $\sigma_R^{N_2}(z, \pi)$ is a known function (e.g., from standard atmospheric models).

This technique has a significant advantage over the elastic scattering technique, whereas, instead of two variables (the aerosol backscattering and extinction coefficients), only one variable is unknown, namely, the aerosol extinction coefficient, which is easily found from Eq. (4.11). The backscattering coefficient is then found as a ratio of elastic lidar return to Raman one. In this way the problem uncertainty (lidar ratio) is significantly reduced. However, the appearing drawback is a logarithmic derivative, which in the presence of experimental errors is a mathematically incorrect procedure and needs regularization.

4.2.4 The Raman DIAL method

Raman DIAL method is analogous to the conventional DIAL method, but, instead of two elastic lidar returns at different wavelengths, one Raman lidar return is used (Reichardt et al., 1996; Tomasi et al., 2001). This method is generally used to measure the concentration of gases in atmosphere. Raman scattering is from nitrogen or oxygen (or both), and the wavelengths are tuned in such a way that the initial wavelength matches the absorption band of the gas to be investigated and the shifted wavelength matches the band where the atmosphere is clear.

Thus, for example, when investigating the ozone profile, the initial wavelength is set in the near-UV, where ozone absorption is strong, while the shifted wavelength reaches the visible range, where atmosphere does not absorb sensibly.

Lidar return is written in the form:

$$F(z) = A \sigma_R^{N_2}(z, \pi) \exp\left(-\int_0^z \alpha^{O_3}(z', \lambda_0) dz' - 2 \int_0^z \sigma(z') dz'\right), \quad (4.12)$$

where α^{O_3} is the ozone absorption coefficient:

$$\alpha^{O_3} = Q_a^{O_3}(\lambda_0) n^{O_3}(z), \quad (4.13)$$

where $Q_a^{O_3}$ is the absorption cross-section of an ozone molecule.

So, the concentration $n^{O_3}(z)$ can be easily found:

$$n^{O_3}(z) = -\frac{1}{Q_a^{O_3}(\lambda_0)} \left\{ \frac{d}{dz} \ln \left(\frac{F(z)}{A \sigma_R^{N_2}(z, \pi)} \right) + 2\sigma(z) \right\}. \quad (4.14)$$

Reichardt et al. (1996) claim that the Raman DIAL method is less sensitive to measurement errors than the conventional DIAL method and, therefore, it is much more accurate. The Raman DIAL method is even more stable, if one measures the ratio of Raman signals from two stable components of atmosphere, namely nitrogen and oxygen.

4.2.5 The method of rotational Raman scattering for determining the thermodynamic characteristics of atmosphere

The use of the rotational spectrum of Raman scattering as a way of measuring temperature was apparently suggested first by Cooney (1972). In most cases of Raman lidar sounding of atmosphere the frequency shift, corresponding to the main vibrational transition, is used. The energy of vibrational transition is much greater than the energy of heat motion of molecules. This makes the vibrational transition signal independent of temperature and, therefore, convenient to use as a reference. The energy of pure-rotational transition, on the other hand, is of the same order of the heat motion energy and, therefore, the rotational transition signal can be used to measure temperature profile (Mattis et al., 2002).

Let, for example, one measure two rotational Raman scattering signals, corresponding to the quantum numbers j_1 and j_2 :

$$F_R^{j_1}(z) = A \sigma_R^{N_2}(j_1, z, \pi) \exp\left(-\int_0^z [\varepsilon(z', \lambda_0) + \varepsilon(z', \lambda_R^{j_1})] dz'\right), \quad (4.15)$$

$$F_R^{j_2}(z) = A \sigma_R^{N_2}(j_2, z, \pi) \exp\left(-\int_0^z [\varepsilon(z', \lambda_0) + \varepsilon(z', \lambda_R^{j_2})] dz'\right). \quad (4.16)$$

Whereas the frequency shift at rotational transition is much less than that at vibrational transition, in this case the difference between extinction coefficients at initial and shifted wavelengths can be neglected. So, the ratio of signals (4.15) and (4.16) gives:

$$\frac{F_R^{j_1}(z)}{F_R^{j_2}(z)} = \frac{\sigma_R^{N_2}(j_1, z, \pi)}{\sigma_R^{N_2}(j_2, z, \pi)}, \quad (4.17)$$

where the ratio of scattering coefficients is proportional to the ratio of concentrations of molecules, belonging to different energy levels, and is described with the Boltzmann distribution:

$$\frac{F_R^{j_1}(z)}{F_R^{j_2}(z)} = \exp\left(\frac{C_1}{T(z)} + C_2\right). \quad (4.18)$$

Constants C_1 and C_2 are usually found through calibration of lidar data with that of a radiosonde. The temperature profile is then found from the formula:

$$T(z) = \frac{C_1}{\ln\left(F_R^{j_1}(z)/F_R^{j_2}(z)\right) - C_2}. \quad (4.19)$$

It is interesting to note that due to negligible frequency shift the method of rotational Raman scattering is not affected in most cases by multiple scattering.

4.3 The Raman lidar return with regard to multiple scattering

4.3.1 Problem statement

Let us consider the following problem. The sounding medium is a plane-parallel turbid layer. A lidar is located at the distance H from the nearest border of a layer. We use the Cartesian coordinate system with the OZ axis, perpendicular to the border and directed into the medium. The two-dimensional vector \mathbf{r} describes the coordinates in the plane (x, y) . The two-dimensional vector \mathbf{n} is a projection of a unit vector, pointing the direction of light propagation, onto the plane (x, y) . The lidar is situated at the point $(-H, 0, 0)$. The spatial-angular distribution of the source radiance and the diagram of the receiver sensitivity are given by functions $\varphi_{\text{src}}(\mathbf{r}, \mathbf{n})$ and $\varphi_{\text{rec}}(\mathbf{r}, \mathbf{n})$, which are normalized as following:

$$\int \varphi_{\text{src}}(\mathbf{r}, \mathbf{n}) \, d\mathbf{r} \, d\mathbf{n} = 1, \quad (4.20)$$

$$\int \varphi_{\text{rec}}(\mathbf{r}, \mathbf{n}) \, d\mathbf{r} \, d\mathbf{n} = S_{\text{rec}} \Omega_{\text{rec}}, \quad (4.21)$$

where S_{rec} and Ω_{rec} are the area and the solid angle of the receiver, respectively.

The scattering medium is characterized by the extinction coefficient $\varepsilon(\lambda, z)$, the elastic scattering coefficient $\sigma(\lambda, z)$, the elastic scattering phase function $P(\lambda, \theta)$, the Raman scattering coefficient σ_R (total), and the Raman scattering phase function $P_R(\theta)$. Phase functions are normalized as:

$$\frac{1}{2} \int_0^\pi P(\theta) \sin \theta \, d\theta = 1. \quad (4.22)$$

The initial wavelength is λ_0 , the Raman shifted wavelength is λ_R that is defined by Eq. (4.4).

4.3.2 General solution

The model of small-angle quasi-single scattering, which accounts for multiple forward scattering and single backward scattering, has been successfully used to describe multiple scattering in elastic lidar sounding (Katsev et al., 1997; Zege et al., 1995). This approach is bound up with the fact that phase functions of real geophysical media, such as clouds, aerosols, and seawater, are strongly peaked in the forward direction. As a result, the angular spectrum of scattered light from a laser source is peaked in the forward direction too. This means that in most of the problems of lidar sounding one can consider just the only one event of scattering to large angles. According to this approximation, the expression for the lidar return has a form (Katsev et al., 1997):

$$F(z) = W_0 \frac{\sigma(\lambda, z)}{4\pi} \int d\mathbf{r} d\mathbf{n}' d\mathbf{n}'' I_{\text{src}}(z, \mathbf{r}, \mathbf{n}') P(z, \pi - |\mathbf{n}' - \mathbf{n}''|) I_{\text{rec}}(z, \mathbf{r}, \mathbf{n}''), \quad (4.23)$$

where W_0 is a laser pulse energy, $I_{\text{src}}(z, \mathbf{r}, \mathbf{n})$ and $I_{\text{rec}}(z, \mathbf{r}, \mathbf{n})$ are the angular distributions of the radiance at the point (z, \mathbf{r}) , due to the *real* and *fictitious* continuous wave sources of unit power with the spatial-angular diagrams $\varphi_{\text{src}}(\mathbf{r}, \mathbf{n})$ and $\varphi_{\text{rec}}(\mathbf{r}, \mathbf{n})$, respectively. Functions $I_{\text{src}}(z, \mathbf{r}, \mathbf{n})$ and $I_{\text{rec}}(z, \mathbf{r}, \mathbf{n})$ satisfy the radiative transfer equation and can be found within the small-angle approximation.

A real lidar records temporal dependencies of the lidar return power $F(t)$, t being the photon arrival time. This approach neglects the temporal spread of small-angle photons and associates the photon arrival time t with the depth z , which the photons return from, by Eq. (4.2). As a matter of fact, the forward pulse stretching can violate the relation (4.2) and affect the lidar return (McLean et al., 1998). However, both theoretical estimations and computer simulations show that this feature has to be regarded only for sounding layers of large optical thicknesses (Zege et al., 2001).

In order to find the Raman lidar return under strong influence of multiple scattering, we should note first that the Raman scattering coefficient is several orders less than the elastic scattering coefficient, for example, for clouds, their ratio is about 10^{-6} or even less (Reichardt et al., 1996). This means that only one Raman scattering event is enough to account for. On the contrary, the elastic scattering should be considered as multiple one.

By the manner of forming light field, elastic scattering can be divided into small-angle scattering and backward (large-angle) scattering. According to Katsev et al. (1997), because of the forward peak of elastic scattering, backscattering can be considered just once in lidar sounding. Hence, multiple scattering appears in small-angle elastic scattering only.

Having separated in such a way the process of forming light field into forward elastic multiple scattering (FES), backward elastic scattering (BES), forward Raman scattering (FRS), and backward Raman scattering (BRS), and considering just one event of Raman and one event of backward elastic scattering, we arrive at the conclusion that the Raman lidar return could be formed by the following processes:

1. FES – BRS – FES,
2. FES – FRS – FES – BES – FES,
3. FES – BES – FES – FRS – FES.

The second and the third processes are obviously equivalent, so we will merge them into one process: forward Raman – backward elastic (FRS – BES). The first process is principally different: it includes the Raman backscattering event and there is no elastic backscattering in it. As it happens, the FRS – BES process can be neglected comparing to the first process (BRS). Let us display it, using the double-scattering pattern. The relative contribution of double-scattering $F^{(2)}(z)$, as compared with the single scattering $F^{(1)}(z)$, in the case of a homogeneous medium equals (Cohen et al., 1978; Eloranta, 1972; Samokhvalov, 1979):

$$\frac{F^{(2)}(z)}{F^{(1)}(z)} = \frac{\sigma(\lambda)(z+H)}{P(\pi)} \gamma_{\text{rec}} \int_0^{\pi/2} P(\gamma)P(\pi-\gamma) d\gamma, \quad (4.24)$$

where γ_{rec} is the receiver field-of-view (FOV).

Here we imply that the source is a mono-directional one and FOV is small enough:

$$\frac{z+H}{z} \gamma_{\text{rec}} \ll 1. \quad (4.25)$$

Noting that in our case double scattering consists of one elastic and one Raman scattering event, we get:

$$\begin{aligned} \frac{F^{(\text{el},R)}(z)}{F^{(R)}(z)} = \frac{(z+H)}{P_R(\pi)} \gamma_{\text{rec}} & \left(\sigma(\lambda_R, z) \int_0^{\pi/2} P_R(\gamma)P(\pi-\gamma) d\gamma \right. \\ & \left. + \sigma(\lambda_0, z) \int_0^{\pi/2} P(\gamma)P_R(\pi-\gamma) d\gamma \right). \quad (4.26) \end{aligned}$$

The first term in parentheses describes the FRS – BES process, and the second one describes the BRS process. The ratio of these two terms illustrates the contribution of the FRS – BES process, in comparison with the BRS process. This ratio can be estimated as a ratio of elastic phase function integral over backward hemisphere to that over forward hemisphere:

$$\int_{\pi/2}^{\pi} P(\gamma) d\gamma / \int_0^{\pi/2} P(\gamma) d\gamma.$$

This ratio is negligible for real geophysical media, because of the forward scattering peak. It is about 10^{-3} for the Cloud C.1 model (Deirmendjian, 1969) in the visible range.

So, the process FES – BRS – FES is the main contribution to light field forming. Or, if we decode it, light field forming goes the following way (see Fig. 4.1):

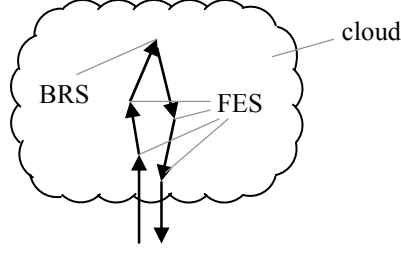


Fig. 4.1. The scheme of forming the Raman lidar return.

1. elastic small-angle multiple scattering, when photons travel out of the lidar into the medium,
2. the single event of Raman scattering in the backward direction,
3. elastic (but at the shifted wavelength) small-angle multiple scattering, when photons travel from the medium back to the lidar.

This scheme is a complete paradigm of the model (4.23) for elastic lidar sounding.

Thus the model (4.23) can be easily generalized to the case of Raman lidar sounding. To do so, one should

- replace the elastic scattering coefficient $\sigma(\lambda, z)$, followed by the integral, by the Raman scattering coefficient $\sigma_R(z)$,
- substitute the Raman scattering phase function $P_R(\pi - \theta)$ for the elastic backscattering phase function $P(\pi - \theta)$,
- use medium characteristics at wavelengths λ_0 and λ_R , while calculating functions $I_{\text{src}}(z, \mathbf{r}, \mathbf{n})$ and $I_{\text{rec}}(z, \mathbf{r}, \mathbf{n})$, respectively.

Finally we get the expression for the Raman lidar return:

$$F_R(z) = W_0 \frac{\sigma_R(z)}{4\pi} \int d\mathbf{r} d\mathbf{n}' d\mathbf{n}'' I_{\text{src}}(\lambda_0, z, \mathbf{r}, \mathbf{n}') P_R(\pi - |\mathbf{n}' - \mathbf{n}''|) I_{\text{rec}}(\lambda_R, z, \mathbf{r}, \mathbf{n}''). \quad (4.27)$$

This expression can be rewritten more compactly by introducing the effective light field radiance:

$$I_{\text{eff}}(z, \mathbf{r}, \mathbf{n}) = \int d\mathbf{r}' d\mathbf{n}' I_{\text{src}}(\lambda_0, z, \mathbf{r}', \mathbf{n}') I_{\text{rec}}(\lambda_R, z, \mathbf{r} + \mathbf{r}', \mathbf{n} + \mathbf{n}'). \quad (4.28)$$

Then Eq. (4.27) can be presented as:

$$F_R(z) = W_0 \frac{\sigma_R(z)}{4\pi} \int d\mathbf{n} P_R(\pi - |\mathbf{n}|) I_{\text{eff}}(z, \mathbf{r} = 0, \mathbf{n}). \quad (4.29)$$

This expression is more compact and demonstrative. However we need to figure out the physical meaning of the effective radiance I_{eff} .

To do so, let us introduce the Fourier transform of the function I_{eff} and the Hankel transform of the Raman backscattering function $P_R(\pi - \theta)$:

$$I_{\text{eff}}(z, \boldsymbol{\nu}, \mathbf{p}) = \int d\mathbf{r} d\mathbf{n} I_{\text{eff}}(z, \mathbf{r}, \mathbf{n}) \exp(-i\boldsymbol{\nu} \cdot \mathbf{r} - i\mathbf{p} \cdot \mathbf{n}), \quad (4.30)$$

$$P_R(p) = \frac{1}{2} \int_0^\infty P_R(\pi - \theta) J_0(p\theta) \theta d\theta, \quad (4.31)$$

where $J_k(x)$ is the Bessel function of the k th order.

(Here, as always in the small-angle approximation, we assume that backscattering phase function $P_R(\pi - \theta)$ is equal to zero for θ , which is greater than the prescribed value of the scattering angle θ_0 . We choose $\theta_0 = \pi/2$.)

According to the Parseval equality, we have:

$$F_R(z) = W_0 \sigma_R(z) \int \frac{d\boldsymbol{\nu} d\mathbf{p}}{(2\pi)^4} P_R(p) I_{\text{eff}}(z, \boldsymbol{\nu}, \mathbf{p}), \quad (4.32)$$

where

$$I_{\text{eff}}(z, \boldsymbol{\nu}, \mathbf{p}) = I_{\text{src}}^*(\lambda_0, z, \boldsymbol{\nu}, \mathbf{p}) I_{\text{rec}}(\lambda_R, z, \boldsymbol{\nu}, \mathbf{p}). \quad (4.33)$$

Here $I_{\text{src}}(\lambda_0, z, \boldsymbol{\nu}, \mathbf{p})$ and $I_{\text{rec}}(\lambda_R, z, \boldsymbol{\nu}, \mathbf{p})$ are the Fourier transforms of the functions $I_{\text{src}}(\lambda_0, z, \mathbf{r}, \mathbf{n})$ and $I_{\text{rec}}(\lambda_R, z, \mathbf{r}, \mathbf{n})$, respectively (sign * represents complex conjugation).

Within the small-angle approximation, the Fourier transform of light radiance, generated by the source with the diagram $\varphi(\mathbf{r}, \mathbf{n})$ in a scattering medium, is equal to (Zege et al., 1991):

$$I(z, \boldsymbol{\nu}, \mathbf{p}) = \varphi(\boldsymbol{\nu}, \mathbf{p} + \boldsymbol{\nu}(z + H)) \exp\left(-\int_0^z [\varepsilon(\xi) - \sigma(\xi) P^f(|\mathbf{p} + \boldsymbol{\nu}(z - \xi)|)] d\xi\right) \quad (4.34)$$

where $\varphi(\boldsymbol{\nu}, \mathbf{p})$ is the Fourier transform of the source diagram, and $P^f(p)$ is the Hankel transform of the forward scattering phase function:

$$P^f(p) = \frac{1}{2} \int_0^\infty P^f(\theta) J_0(p\theta) \theta d\theta \quad (4.35)$$

Substitution of (4.33) and (4.34) into Eq. (4.32) gives:

$$F_R(z) = W_0 \sigma_R \int \frac{d\boldsymbol{\nu} d\mathbf{p}}{(2\pi)^4} P_R(p) \varphi_{\text{eff}}(\boldsymbol{\nu}, \mathbf{p} + \boldsymbol{\nu}(z + H)) \times \exp\left(-\int_0^z [\varepsilon_{\text{eff}}(\xi) - \sigma_{\text{eff}}(\xi) P_{\text{eff}}^f(|\mathbf{p} + \boldsymbol{\nu}(z - \xi)|)] d\xi\right), \quad (4.36)$$

where

$$\varphi_{\text{eff}}(\boldsymbol{\nu}, \mathbf{p}) = \varphi_{\text{src}}^*(\boldsymbol{\nu}, \mathbf{p}) \varphi_{\text{rec}}(\boldsymbol{\nu}, \mathbf{p}), \quad (4.37)$$

$$\varepsilon_{\text{eff}}(z) = \varepsilon(\lambda_0, z) + \varepsilon(\lambda_R, z), \quad (4.38)$$

$$\sigma_{\text{eff}}(z) = \sigma(\lambda_0, z) + \sigma(\lambda_R, z), \quad (4.39)$$

$$P_{\text{eff}}^f(z, \theta) = \frac{\sigma(\lambda_0, z)P^f(\lambda_0, z, \theta) + \sigma(\lambda_R, z)P^f(\lambda_R, z, \theta)}{\sigma(\lambda_0, z) + \sigma(\lambda_R, z)}. \quad (4.40)$$

So, as seen from (4.36), the effective intensity I_{eff} is the light field radiance, produced by the effective source with the diagram

$$\varphi_{\text{eff}}(\mathbf{r}, \mathbf{n}) = \int d\mathbf{r}' d\mathbf{n}' \varphi_{\text{src}}(\mathbf{r}', \mathbf{n}') \varphi_{\text{rec}}(\mathbf{r}' + \mathbf{r}, \mathbf{n}' + \mathbf{n}) \quad (4.41)$$

in some effective medium with the extinction coefficient, the scattering coefficient, and the forward scattering phase function, defined by Eqs (4.38)–(4.40), respectively.

Formulas (4.36)–(4.41) are the solution of the direct problem of the Raman lidar return simulation within the framework of small-angle approximation. It is to be noted that, unlike other approaches (such as Monte–Carlo (Bruscaglioni et al., 1999) or Shipley (Weinman and Shipley, 1972) methods), this solution explicitly relates the Raman lidar return to the medium optical characteristics and the lidar parameters. This relation is of great importance while solving the inverse problem. Moreover, this approach makes it possible to obtain the solution for the Raman lidar return in the same form as it is for the elastic lidar return. This plays an important role while developing the methods of joint use of the elastic and Raman scattering signals.

4.3.3 Isotropic backscattering approximation

Equation (4.29) can be simplified if one takes into account that the functions in the integrand behave in strongly different ways. Radiance $I_{\text{eff}}(z, \mathbf{r} = 0, \mathbf{n})$ has a sharp peak in the direction $\mathbf{n} = 0$ and is negligible at large angles. In contrast, the Raman phase function is the Rayleigh function (Mobley et al., 1993):

$$P_R(\theta) = \frac{3}{4} \frac{1 + 3w}{1 + 2w} \left(1 + \frac{1 - w}{1 + 3w} \cos^2 \theta \right), \quad (4.42)$$

where w is a depolarization ratio.

The phase function (4.42) is smooth in a neighbourhood of the point $\theta = \pi$ and, therefore, it can be replaced by a constant:

$$P_R(\pi - \theta) \approx P_R(\pi). \quad (4.43)$$

In order to estimate the error of this ‘isotropic’ approximation, let us expand the Rayleigh function into series at the point $\theta = \pi$:

$$P_R(\pi - \theta) \approx P_R(\pi) \left(1 - \frac{1 - w}{1 + w} \frac{\theta^2}{2} \right). \quad (4.44)$$

The relative error δ of changing the function to the isotropic one can be estimated as:

$$\delta = \frac{1-w}{1+w} \frac{\int d\mathbf{n} \frac{\mathbf{n}^2}{2} I_{\text{eff}}(z, \mathbf{r} = 0, \mathbf{n})}{\int d\mathbf{n} I_{\text{eff}}(z, \mathbf{r} = 0, \mathbf{n})}.$$

The ratio of the integrals in this expression is nothing but the variance V_θ of the angular distribution, described by the function $I_{\text{eff}}(z, \mathbf{r} = 0, \mathbf{n})$:

$$V_\theta = \frac{\int d\mathbf{n} \frac{\mathbf{n}^2}{2} I_{\text{eff}}(z, \mathbf{r} = 0, \mathbf{n})}{\int d\mathbf{n} I_{\text{eff}}(z, \mathbf{r} = 0, \mathbf{n})}. \quad (4.45)$$

Hence, the relative error of isotropic approximation is equal to

$$\delta = \frac{1-w}{1+w} V_\theta.$$

Therefore, the isotropic backscattering approximation can be used if

$$\frac{1-w}{1+w} V_\theta \ll 1. \quad (4.46)$$

Let us note that the isotropic approximation requires no restrictions in addition to the small-angle approximation validity condition, which is (Zege et al., 1991):

$$V_\theta \ll 1. \quad (4.47)$$

Computer simulations show that the error of the isotropic approximation is less than 0.03% for a typical geometry of Raman lidar measurements.

So, the expression for the Raman lidar return (4.29) takes the form:

$$F_R(z) = W_0 \sigma_R(\pi) \int d\mathbf{n} I_{\text{eff}}(z, \mathbf{r} = 0, \mathbf{n}), \quad (4.48)$$

where $\sigma_R(\pi)$ is the Raman backscattering coefficient, related to the total Raman scattering coefficient σ_R as following:

$$\sigma_R(\pi) = \frac{\sigma_R P_R(\pi)}{4\pi}. \quad (4.49)$$

It follows in the Fourier space:

$$F_R(z) = W_0 \sigma_R(\pi) \int \frac{d\boldsymbol{\nu}}{(2\pi)^2} I_{\text{eff}}(z, \boldsymbol{\nu}, \mathbf{p} = 0). \quad (4.50)$$

The isotropic approximation results in a strong simplification of expression for the Raman lidar return. The four-dimensional integral in Eq. (4.32) is reduced to the two-dimensional integral in Eq. (4.50), that is of great importance in numeric simulations. Furthermore, the expression (4.48) has a clear physical meaning: the Raman lidar return is proportional to the irradiance on the axis of

the effective light beam in the effective medium with characteristics defined by Eqs (4.38)–(4.40).

So, the problem of the Raman lidar return calculation is reduced to a standard problem of finding the irradiance in a medium with a peaked phase function. A wide range of known small-angle scattering methods could be applied to the solution of this problem (Zege et al., 1991).

4.3.4 The case of axially symmetric source and receiver patterns

A particular case when both source and receiver diagrams have axially symmetric angular-spatial patterns, which can be represented as

$$\varphi_j(\mathbf{r}, \mathbf{n}) = \varphi_j^{\text{sp}}(|\mathbf{r} - \mathbf{r}_j^0|) \varphi_j^{\text{ang}}(|\mathbf{n} - \mathbf{n}_j^0|), \quad j = \text{scr}, \text{rec}, \quad (4.51)$$

is of a great practical interest. In this case, the Fourier transform of the effective source diagram takes the form:

$$\varphi^{\text{eff}}(\boldsymbol{\nu}, \mathbf{p}) = \varphi_{\text{scr}}^{\text{sp}}(\nu) \varphi_{\text{scr}}^{\text{ang}}(p) \varphi_{\text{rec}}^{\text{sp}}(\nu) \varphi_{\text{rec}}^{\text{ang}}(p) \exp(-i \boldsymbol{\nu} \cdot \mathbf{R} - i \mathbf{p} \cdot \boldsymbol{\Omega}), \quad (4.52)$$

where $\mathbf{R} = \mathbf{r}_{\text{rec}}^0 - \mathbf{r}_{\text{scr}}^0$ is the vector, connecting the source and receiver centres, $\boldsymbol{\Omega} = \mathbf{n}_{\text{rec}}^0 - \mathbf{n}_{\text{scr}}^0$ is the vector, determining the angle between the receiver and source axes. Besides, it follows:

$$\begin{aligned} \varphi_j^{\text{ang}}(p) &= 2\pi \int_0^\infty \varphi_j^{\text{ang}}(\theta) J_0(p\theta) \theta \, d\theta, \\ \varphi_j^{\text{sp}}(\nu) &= 2\pi \int_0^\infty \varphi_j^{\text{sp}}(r) J_0(\nu r) r \, dr; \quad j = \text{scr}, \text{rec}. \end{aligned} \quad (4.53)$$

Equation (4.52) makes possible the simplification of the expression (4.50) by integrating over the azimuth and reducing the integral (4.50) to the one-dimensional integral:

$$F_R(z) = W_0 \sigma_R(\pi) \int \frac{\nu \, d\nu}{2\pi} J_0(\nu |\mathbf{R} + (z + H)\boldsymbol{\Omega}|) I_{\text{eff}}(z, \nu, \mathbf{p} = 0). \quad (4.54)$$

Here, the Fourier transform of the effective intensity is:

$$I_{\text{eff}}(z, \nu, \mathbf{p} = 0) = \varphi'(\nu, \nu(z + H)) \exp\left(-\int_0^z [\varepsilon_{\text{eff}}(\xi) - \sigma_{\text{eff}}(\xi) P_{\text{eff}}^f(\nu(z - \xi))] \, d\xi\right) \quad (4.55)$$

and

$$\varphi'(\nu, p) = \varphi_{\text{scr}}^{\text{sp}}(\nu) \varphi_{\text{scr}}^{\text{ang}}(p) \varphi_{\text{rec}}^{\text{sp}}(\nu) \varphi_{\text{rec}}^{\text{ang}}(p). \quad (4.56)$$

Equations (4.51)–(4.56), along with the effective medium properties (4.38)–(4.40), give the explicit solution to the problem for the case of axially symmetric source and receiver patterns.

Figure 4.2 presents the Raman lidar return simulation example in comparison with the data of Wandinger (1998).

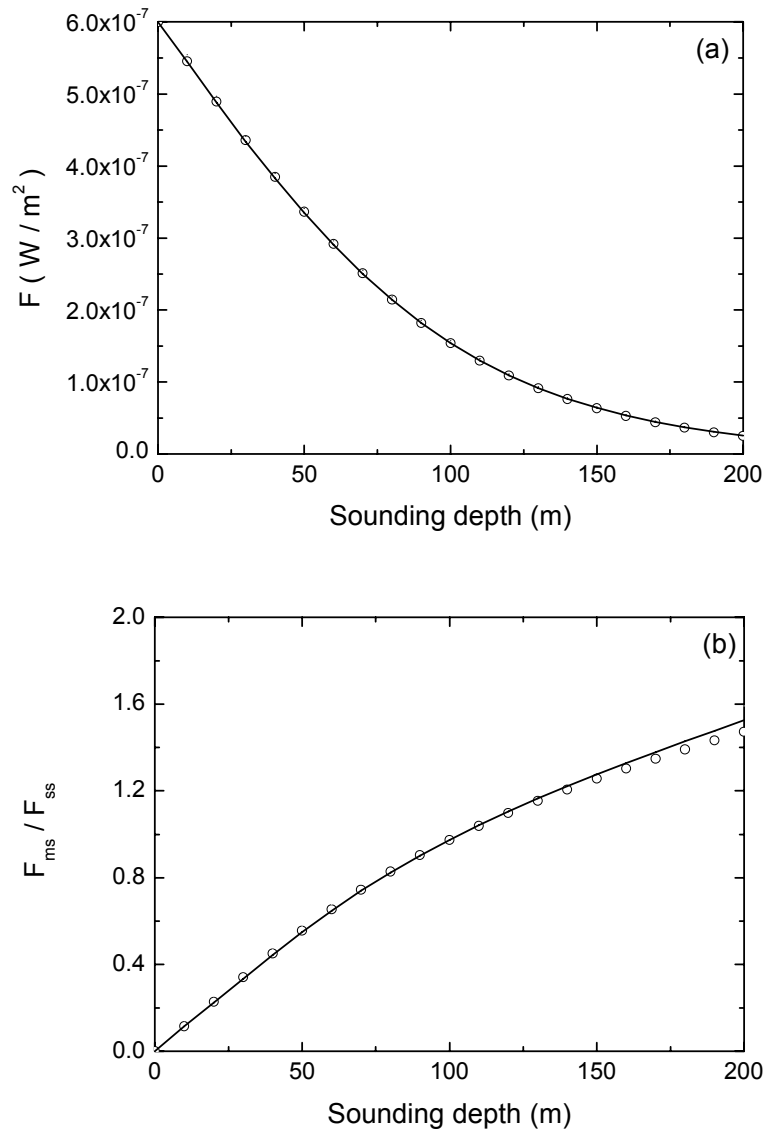


Fig. 4.2. The total signal (a) and the multiple-to-single scattering ratio (b). Data by Wandinger (1998) (\circ) and the solution (4.54) (curve). The cloud C.1 model (Deirmendjian, 1969) with an extinction coefficient of 0.01 m^{-1} . The lidar-cloud distance is 5000 m , the source divergence is 0.1 mrad , the receiver's FOV is 0.4 mrad (full angles).

4.4 Spatial-angular pattern of the Raman lidar return

4.4.1 Introduction to the problem

The Raman lidar return is usually used in the sounding of aerosols to measure the extinction coefficient profile, because within the framework of the single scattering approximation the Raman lidar return depends on the extinction coefficient alone. Owing to the spectral dependence of the extinction coefficient, the microstructure characteristics of a medium (e.g., sizes of particles) can be retrieved. However, for the sounding of clouds, consisting of large particles, the spectral behaviour of the extinction coefficient contains no information about microstructure parameters. On the other hand, when sounding clouds, the effect of multiple scattering becomes significant, and lidar return depends not only on the extinction, but also on the phase function, which, in its turn, depends on the size of the scatterers.

Multiple scattering becomes crucial when measuring angular patterns of lidar return (e.g., with a multiple-field-of-view (Bissonnette and Hutt, 1990) or imaging (Muscarelli et al., 1996) receiver). In that case the signal at some angles is exclusively determined by multiple scattering.

Bissonnette and Hutt (1990) and Roy et al. (1997) apparently were the first to suggest using a multiple-field-of-view (MFOV) receiver to determine the effective particle size using elastic lidar sounding of warm clouds and aerosols. However, the absence of the appropriate theoretical base made them use the semi-empirical methods in the retrieval procedure. The theoretical investigation of an angular pattern of the elastic lidar return from warm clouds is given by Polonsky et al. (2001). This investigation shows that for sounding depths, at which the scattering is mainly determined by Fraunhofer diffraction on water droplets, the angular dependence of the lidar return appears as a product of the receiving angle by the effective droplet size. Such an angular dependence enables the retrieval of cloud droplet sizes. However, the complex behaviour of the elastic backscattering phase function hinders the implementation of such methods (e.g., accounting for finite size of the receiver, which is necessary when investigating the spatial-angular pattern of lidar return). In fact, isotropic backscattering simplifies the problem greatly for the case of Raman lidar sounding.

Basing on the developed model, the investigation of spatial-angular pattern of the Raman lidar return is carried out in this chapter. Further, on its basis, a new optical particle sizing technique is proposed.

4.4.2 The effective medium properties

In order to investigate the spatial-angular pattern of the Raman lidar return, let us examine first the properties of the effective medium introduced above. We consider optically hard scatterers of sizes much larger than the wavelength. Warm (liquid) clouds could be a paradigm of such a medium. Further, we consider sounding depths that are not very large. These two premises allow us to regard scattering as Fraunhofer diffraction of light on water droplets. Within

the framework of the Fraunhofer diffraction approximation the scattering cross-section and, therefore, the scattering coefficient σ^D do not depend on wavelength:

$$\sigma^D(\lambda_0, z) = \sigma^D(\lambda_R, z) = \sigma^D(z). \quad (4.57)$$

So the effective phase function (4.40) is:

$$P_{\text{eff}}^D(\theta) = \frac{P^D(\lambda_0, \theta) + P^D(\lambda_R, \theta)}{2}, \quad (4.58)$$

where $P^D(\lambda, \theta)$ is the Fraunhofer phase function (van de Hulst, 1957):

$$P^D(\lambda, \theta) = \frac{1}{\langle r^2 \rangle} \left\langle r^2 \frac{4}{\theta^2} J_1^2 \left(\frac{2\pi r}{\lambda} \theta \right) \right\rangle, \quad (4.59)$$

where r is a droplet radius (angle brackets denote size averaging).

As was shown by Kokhanovsky and Zege (1997), the phase function of clouds does not really depend on the exact form of the size distribution function, but rather on the value of the effective diffraction parameter (the dimensionless droplets size) ρ_{32} defined as:

$$\rho_{32} = \frac{2\pi r_{32}}{\lambda}, \quad (4.60)$$

where r_{32} is the effective droplets radius:

$$r_{32} = \frac{\langle r^3 \rangle}{\langle r^2 \rangle} \quad (4.61)$$

and λ is the wavelength of the incident light.

As a result, whereas the angular dependence in Fraunhofer diffraction appears as a product $\rho\theta$, $\rho = 2\pi a/\lambda$ being the dimensionless radius of scatterers, the diffraction phase function should have the form:

$$P^D(\theta) = \rho_{32}^2 \Phi(\rho_{32}\theta), \quad (4.62)$$

where the function $\Phi(x)$ satisfies the normalizing condition, which is the small-angle analogue of Eq. (4.22):

$$\frac{1}{2} \int_0^\infty \Phi(x) x \, dx = 1. \quad (4.63)$$

According to the developed model, the light propagates into the medium at the initial wavelength and travels back to the lidar receiver at the shifted wavelength. Hence, with application to Raman lidar sounding, we can introduce the effective dimensionless radius:

$$\rho_{\text{eff}} = \frac{1}{2} (\rho_{32}(\lambda_0) + \rho_{32}(\lambda_R)) = \frac{\pi r_{32}}{\lambda_0} + \frac{\pi r_{32}}{\lambda_R}, \quad (4.64)$$

and, thereafter, the effective wavelength λ_{eff} :

$$\frac{2}{\lambda_{\text{eff}}} = \frac{1}{\lambda_0} + \frac{1}{\lambda_R}. \quad (4.65)$$

Then it follows:

$$\rho_{\text{eff}} = \frac{2\pi r_{32}}{\lambda_{\text{eff}}}. \quad (4.66)$$

Taking into account that λ_R is related to λ_0 and $\delta\tilde{\nu}$ through Eq. (4.4), let us express the initial and shifted wavelengths through λ_{eff} :

$$\lambda_{0,R} = \frac{\lambda_{\text{eff}}}{1 \pm \lambda_{\text{eff}}\delta\tilde{\nu}/2}. \quad (4.67)$$

As could be easily shown by differentiation with respect to parameter ρ_{32} , the phase function value at the point $\theta = 0$, in the case of a fairly wide size distribution, is most sensitive to the size of scatterers, and, therefore, to the wavelength. It follows from Eq. (4.59) that:

$$P^D(\lambda, \theta = 0) = \frac{4\pi^2}{\lambda^2} \frac{\langle r^4 \rangle}{\langle r^2 \rangle} \quad (4.68)$$

and one can derive at $\theta = 0$ (see Eq. (4.58)):

$$\begin{aligned} \frac{P^D(\lambda_0, 0) + P^D(\lambda_R, 0)}{2} &= 2\pi^2 \frac{\langle r^4 \rangle}{\langle r^2 \rangle} \left(\frac{1}{\lambda_0^2} + \frac{1}{\lambda_R^2} \right) \\ &= 2\pi^2 \frac{\langle r^4 \rangle}{\langle r^2 \rangle} \left(\frac{(1 + \lambda_{\text{eff}}\delta\tilde{\nu}/2)^2}{\lambda_{\text{eff}}^2} + \frac{(1 - \lambda_{\text{eff}}\delta\tilde{\nu}/2)^2}{\lambda_{\text{eff}}^2} \right) \\ &= \frac{4\pi^2}{\lambda_{\text{eff}}^2} \frac{\langle r^4 \rangle}{\langle r^2 \rangle} \left(1 + \left(\frac{\lambda_{\text{eff}}\delta\tilde{\nu}}{2} \right)^2 \right) \\ &= P^D(\lambda_{\text{eff}}, 0) \left(1 + \left(\frac{\lambda_{\text{eff}}\delta\tilde{\nu}}{2} \right)^2 \right). \end{aligned} \quad (4.69)$$

That is, the half-sum of the Fraunhofer phase functions at $\theta = 0$ equals the Fraunhofer phase function at the effective wavelength within accuracy to the second order of the value $\lambda_{\text{eff}}\delta\tilde{\nu}$. If the initial wavelength is 532 nm and Raman scattering is from nitrogen, the shifted wavelength will be 607 nm and the effective one will be 567 nm. In this case the correction will be less than 1%. (For Raman lidar sounding the shorter wavelengths are often used. In that case the correction is even smaller, for example, for the initial wavelength of 308 nm it is about 0.1%.) Whereas the phase function value at $\theta = 0$ is most sensitive to the wavelength, the effective phase function (4.58) can be changed by the phase function at the effective wavelength for any θ with a correction less than the correction for $\theta = 0$. Finally, we get:

$$P_{\text{eff}}^D(\theta) = P^D(\lambda_{\text{eff}}, \theta) = \rho_{\text{eff}}^2 \Phi(\rho_{\text{eff}}\theta). \quad (4.70)$$

Thus, the effective forward scattering phase function depends on the effective dimensionless radius only.

It should be noted that the effective dimensionless radius and, therefore, the phase function can generally depend on the sounding depth z . However, in order to simplify the problem, we will consider here the case when ρ_{eff} does not depend on z , otherwise, the effective particle size will stand for some average value over the interval $(0, z)$.

4.4.3 Spatial-angular patterns of Raman lidar returns and their dependence on the size of scatterers

Now, after investigating the angular pattern of the effective medium phase function, let us consider the pattern of a lidar return.

Let a source be infinitesimal and mono-directional, i.e., its diagram is:

$$\varphi_{\text{src}}(\mathbf{r}', \mathbf{n}') = \delta(\mathbf{r}')\delta(\mathbf{n}'), \quad (4.71)$$

where $\delta(\mathbf{x})$ is the two-dimensional Dirac δ -function.

Let us investigate the spatial-angular distribution of returned radiance in the lidar plane ($z = -H$). This means that the 'receiver' has a diagram:

$$\varphi_{\text{rec}}(\mathbf{r}', \mathbf{n}') = \delta(\mathbf{r}' - \mathbf{r})\delta(\mathbf{n}' - \mathbf{n}), \quad (4.72)$$

and its Fourier transform is equal to:

$$\varphi_{\text{rec}}(\boldsymbol{\nu}, \mathbf{p}) = \exp(-i\boldsymbol{\nu} \cdot \mathbf{r} - i\mathbf{p} \cdot \mathbf{n}). \quad (4.73)$$

Then, the diagram of the effective source (4.41) is identical to the diagram (4.72) and its Fourier transform is given by (4.73). The Raman lidar return, according to Eq. (4.48), is proportional to the irradiance, produced by this source in the effective medium at the point $(z, 0, 0)$. Substituting (4.70) and (4.73) into (4.48) and keeping in mind that the scattering coefficient does not depend on wavelength, we get, after integrating over the azimuth:

$$\begin{aligned} F(z, \mathbf{r}, \mathbf{n}) &= W_0 \sigma_R(\pi) \int \frac{\nu d\nu}{2\pi} J_0(\nu|\mathbf{r} + \mathbf{n}(z + H)|) \\ &\times \exp\left(-\int_0^z [\varepsilon_{\text{eff}}(\xi) - 2\sigma^D(\xi)P_{\text{eff}}^D(\nu(z - \xi))] d\xi\right). \end{aligned} \quad (4.74)$$

Here $P_{\text{eff}}^D(p)$ is the Hankel transform of the diffraction phase function $P_{\text{eff}}^D(\theta)$:

$$\begin{aligned} P_{\text{eff}}^D(p) &= \frac{1}{2} \int_0^\infty \rho_{\text{eff}}^2 \Phi(\rho_{\text{eff}}\theta) J_0(p\theta) \theta d\theta \\ &= \frac{1}{2} \int_0^\infty \Phi(x) J_0\left(x \frac{p}{\rho_{\text{eff}}}\right) x dx = \chi(p/\rho_{\text{eff}}), \end{aligned} \quad (4.75)$$

where $\chi(p)$ is the Hankel transform of the function $\Phi(x)$.

Substituting (4.75) into (4.74) and changing variables in integration

$$\boldsymbol{\nu} \rightarrow \rho_{\text{eff}}\boldsymbol{\nu},$$

we come to the expression

$$F(z, \mathbf{r}, \mathbf{n}) = W_0 \sigma_R(\pi) \rho_{\text{eff}}^2 \int \frac{\nu d\nu}{2\pi} J_0(\rho_{\text{eff}} \nu |\mathbf{r} + \mathbf{n}(z + H)|) \times \exp\left(-\int_0^z [\varepsilon_{\text{eff}}(\xi) - 2\sigma^D(\xi)\chi(\nu(z - \xi))] d\xi\right), \quad (4.76)$$

in which spatial and angular coordinates appear as a combination $\rho_{\text{eff}}|\mathbf{r} + (z + H)\mathbf{n}|$ only:

$$F(z, \mathbf{r}, \mathbf{n}) = \rho_{\text{eff}}^2 f(\rho_{\text{eff}}|\mathbf{r} + (z + H)\mathbf{n}|). \quad (4.77)$$

If the receiver size is negligible, its spatial diagram is:

$$\varphi_{\text{rec}}(\mathbf{r}) = S_{\text{rec}} \delta(\mathbf{r}). \quad (4.78)$$

In that case one can put $\mathbf{r} = 0$ in Eq. (4.77) and find that the lidar return does not depend on the azimuth, but only on the product of ρ_{eff} by the receiving angle θ :

$$F(z, \theta) = \rho_{\text{eff}}^2 f((z + H)\rho_{\text{eff}}\theta). \quad (4.79)$$

To illustrate the accuracy of Eq. (4.79) we simulated the angular distribution of the Raman lidar return on the basis of the initial expression (4.54) without additional approximations. The phase functions were calculated with Mie theory for warm clouds with droplets size distribution of Cloud C.1 type (Deirmendjian, 1969) with different effective radii r_{32} :

$$\frac{d\omega}{dr} = \frac{r^m}{m!} \left(\frac{r_{32}}{m+3}\right)^{-m-1} \exp\left(-\frac{r(m+3)}{r_{32}}\right), \quad (4.80)$$

where r is the droplet radius, $d\omega$ is the probability that the droplet radius lies in the interval from r to $r + dr$, m is a Gamma-distribution parameter (here $m = 6$).

The dependence of the ratio $F(z, \theta)/\rho_{\text{eff}}^2$ on the product $\rho_{\text{eff}}\theta$ is plotted in Fig. 4.3. The initial wavelength is 532 nm, the shifted one is 607 nm (the effective one is 567 nm). The cloud altitude is 1000 m, the receiver radius is 25 cm, and the pulse energy is 1 J. It is seen that, regardless of great difference in properties of media under consideration (the effective radius varies all over the range usually observed in warm clouds), the value $F(z, \theta)/\rho_{\text{eff}}^2$ depends on the product $\rho_{\text{eff}}\theta$ only, in close agreement with Eq. (4.79). The discrepancy in the range of small angles is due to the singly scattered light, for which the approximation (4.78) is inapplicable.

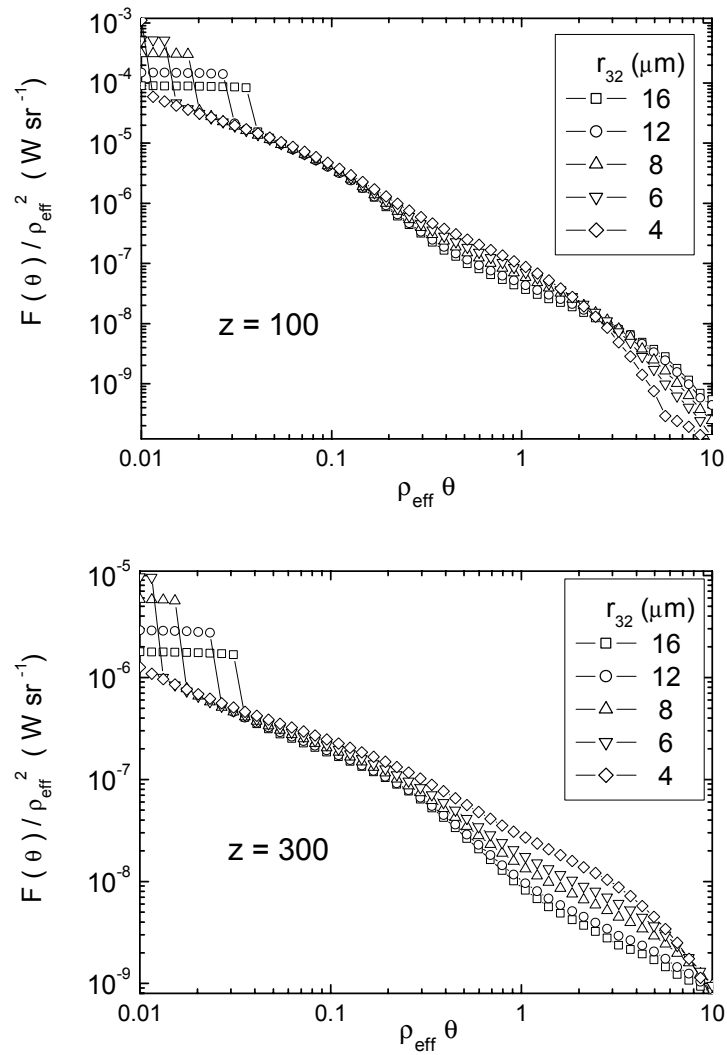


Fig. 4.3. Ratio $F(z, \theta) / \rho_{\text{eff}}^2$ vs. the product $\rho_{\text{eff}} \theta$ for clouds with the different effective size of droplets.

4.5 Retrieval of the microphysical properties of light scattering media using measurements of the Raman lidar return angular patterns

4.5.1 The retrieval possibilities

Equation (4.79) makes it possible to determinate the sizes of scatterers using measurements of the Raman lidar return at several angular intervals. Indeed, integrating (4.76) over the spatial coordinate from 0 to R and over the angle from 0 to γ , we get:

$$F(\gamma) = W_0 \sigma_R(\pi) \frac{R\gamma}{z+H} \int \frac{2\pi d\nu}{\nu} J_1(\rho_{\text{eff}} R \nu) J_1(\rho_{\text{eff}}(z+H)\gamma \nu) \times \exp\left(-\int_0^z [\varepsilon_{\text{eff}}(\xi) - 2\sigma^D(\xi)\chi(\nu(z-\xi))] d\xi\right), \quad (4.81)$$

where $F(\gamma)$ denotes the light flux, measured with the receiver of radius R at the angle interval from 0 to γ :

$$F(\gamma) = \int_0^\gamma \theta d\theta \int_0^{2\pi} d\phi^{\text{ang}} \int_0^R r dr \int_0^{2\pi} d\phi^{\text{sp}} F(z, \mathbf{r}, \mathbf{n}), \quad (4.82)$$

where ϕ^{ang} , ϕ^{sp} is the azimuthal angle for angular and spatial coordinates, respectively.

According to Eq. (4.81), FOV γ , the receiver radius R , and the effective dimensionless radius ρ_{eff} appear in this expression only as a combination:

$$F(\gamma) = R\gamma f(\rho_{\text{eff}} R, \rho_{\text{eff}} \gamma). \quad (4.83)$$

Then the ratio of the flux F_1 , measured in the interval (γ_0, γ_1) , to the flux F_0 , measured in the interval $(0, \gamma_0)$ depends on the two cloud characteristics only: ρ_{eff} and the scattering coefficient σ^D :

$$\frac{F_1}{F_0} = \frac{F(\gamma_1) - F(\gamma_0)}{F(\gamma_0)} = \frac{\gamma_1 f(\rho_{\text{eff}} R, \rho_{\text{eff}} \gamma_1)}{\gamma_0 f(\rho_{\text{eff}} R, \rho_{\text{eff}} \gamma_0)} - 1. \quad (4.84)$$

All other quantities are known values defined by the experiment geometry.

In that case, if the scattering coefficient is known from some other measurements, e.g., through the depth dependence of a lidar return, then the ratio of fluxes $\varsigma = F_1/F_0$ is a function of the single variable ρ_{eff} , which can be easily retrieved by measuring the value of ς .

The dependence of multiply scattered signal on ρ_{eff} is strongest at small angles: the smaller the angle θ , the stronger the dependence. However, at $\theta < R/(z+H)$ the significant portion of the measured signal is the singly scattered light, which contains no information about ρ_{eff} . Therefore, the largest amount

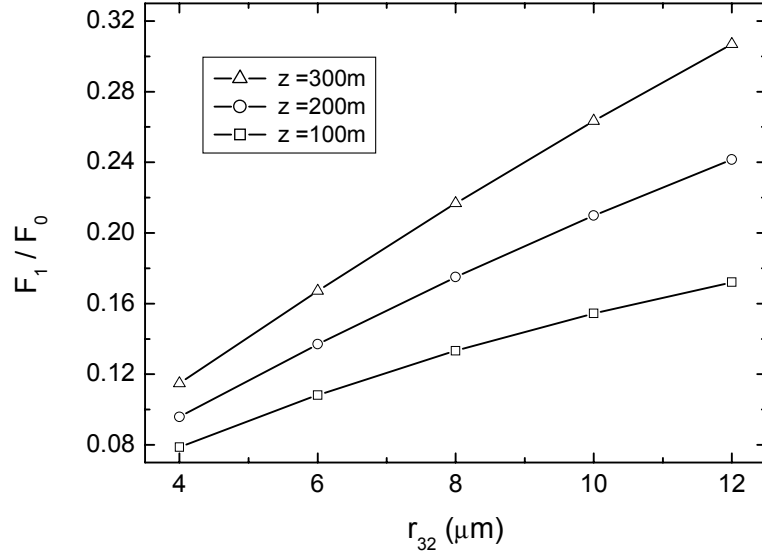


Fig. 4.4. The ratio F_1/F_0 vs. the effective droplets radius.

of information will be carried by a signal measured with an annular receiver at the angular range (γ_0, γ_1) satisfying the conditions:

$$\gamma_1 > \gamma_0 > \frac{R}{z + H}, \quad (4.85)$$

$$\gamma_1 \frac{z + H}{R} - 1 < 1. \quad (4.86)$$

Figure 4.4 presents an example of the dependence of F_1/F_0 on the effective radius of cloud droplets r_{32} for clouds with the particle size distribution (4.80). The calculations were carried out using Eq. (4.54) with no additional approximations. It is evident from Fig. 4.4 that the ratio F_1/F_0 is quite sensitive to the radius of particles, and this sensitivity increases with sounding depth. As it follows from the results presented in the plot, the relative error of retrieving r_{32} has the same order of magnitude as the relative error of measuring the flux ratio F_1/F_0 .

4.5.2 Use of double scattering for retrieving the volume concentration of scatterers

The double-scattering approximation was used by many authors to simulate lidar return (see, for example, Eloranta, 1972; Samokhvalov, 1979). We will consider its small-angle modification and show that for the range of its validity (small FOVs and not very large optical depths), it can be used to retrieve information about a light scattering medium without the use of additional *a priori* data.

Let us consider a homogeneous cloud. In this case the expression for the flux (4.81) takes the form:

$$F(\gamma) = W_0 \sigma_R(\pi) \frac{R\gamma}{z+H} \int \frac{2\pi d\nu}{\nu} J_1(\rho_{\text{eff}} R \nu) J_1(\rho_{\text{eff}}(z+H)\gamma \nu) \times \exp\left(-2\tau + 2\sigma^D \int_0^z \chi(\nu\xi) d\xi\right), \quad (4.87)$$

where τ is the optical depth defined as:

$$\tau = \frac{\varepsilon_{\text{eff}} z}{2}. \quad (4.88)$$

Passing to the dimensionless variables p and η and making the change in Eq. (4.87):

$$\nu = \frac{p}{z}, \quad \xi = \frac{z}{p}\eta, \quad (4.89)$$

we get:

$$F(\gamma) = W_0 \sigma_R(\pi) \frac{R\gamma}{z+H} \int \frac{2\pi dp}{p} J_1\left(\rho_{\text{eff}} \frac{R}{z} p\right) J_1\left(\rho_{\text{eff}} \frac{z+H}{z} \gamma p\right) \times \exp\left(-2\tau + 2\frac{\sigma^D z}{p} \int_0^p \chi(\eta) d\eta\right). \quad (4.90)$$

The double-scattering approximation in the Raman case means that one event of Raman and one event of elastic scattering are taken into account, i.e., one should take the term of the first order of $\sigma^D z$ in Eq. (4.90):

$$F(\gamma) = W_0 \sigma_R(\pi) \frac{R\gamma}{z+H} \int \frac{2\pi dp}{p} J_1\left(\rho_{\text{eff}} \frac{R}{z} p\right) J_1\left(\rho_{\text{eff}} \frac{z+H}{z} \gamma p\right) \times e^{-2\tau} \left(1 + 2\frac{\sigma^D z}{p} \int_0^p \chi(\eta) d\eta\right). \quad (4.91)$$

The unity in the parentheses corresponds to single scattering and the second term corresponds to double scattering, with one forward elastic and one backward Raman scattering event.

The integral (4.91) can be calculated approximately at

$$\rho_{\text{eff}} \frac{z+H}{z} \gamma \ll 1. \quad (4.92)$$

This corresponds to the light field close to the light source. In that case the integral (4.91) is defined by the asymptotic behaviour of the function to be integrated at $p \gg 1$, and the upper limit can be put equal to infinity. This integral can be calculated exactly. To do so, we use Eq. (4.75), according to

which the function $\chi(\eta)$ is the Hankel transform of the function $\Phi(x)$. Then, it follows:

$$\begin{aligned} \int_0^p \chi(\eta) d\eta &\approx \int_0^\infty \chi(\eta) d\eta = \frac{1}{2} \int_0^\infty \Phi(x) dx = \frac{1}{2\rho_{\text{eff}}} \int_0^\infty P_{\text{eff}}^D(\theta) d\theta \\ &= \frac{1}{2\rho_{\text{eff}}} \frac{16}{3\pi} \frac{2\pi}{\lambda_{\text{eff}}} \frac{\langle r^3 \rangle}{\langle r^2 \rangle} = \frac{1}{2\rho_{\text{eff}}} \frac{16}{3\pi} \rho_{\text{eff}} = \frac{8}{3\pi} \end{aligned} \quad (4.93)$$

(when integrating over θ , Eqs (4.59) and (4.70) and also the Parseval equality have been used).

Substituting (4.93) into (4.91), we get:

$$\begin{aligned} F(\gamma) &= W_0 \sigma_R(\pi) \frac{R\gamma}{z+H} \\ &\times \int \frac{2\pi dp}{p} J_1\left(\rho_{\text{eff}} \frac{R}{z} p\right) J_1\left(\rho_{\text{eff}} \frac{z+H}{z} \gamma p\right) e^{-2\tau} \left(1 + \frac{16}{3\pi} \frac{\sigma^D z}{p}\right). \end{aligned} \quad (4.94)$$

Using conditions (4.85), (4.86), and (4.92), and taking the first order of the value $\gamma(z+H)/R - 1$, we get an approximate expression:

$$F(\gamma) = W_0 \sigma_R(\pi) e^{-2\tau} \frac{\pi R^2}{(z+H)^2} \left(1 + \frac{64 \sigma^D \rho_{\text{eff}}}{3\pi^2} ((z+H)\gamma - R/3)\right). \quad (4.95)$$

If the first receiver (circular) measures the signal F_0 in the interval from 0 to γ_0 and the second receiver (annular) measures the signal F_1 in the interval from γ_0 to γ_1 , then the ratio F_1/F_0 is equal to:

$$\frac{F_1}{F_0} = \frac{(z+H)(\gamma_1 - \gamma_0)}{\frac{3\pi^2}{64 \sigma^D \rho_{\text{eff}}} + (z+H)\gamma_0 - R/3}. \quad (4.96)$$

From this equation the product σ^D by ρ_{eff} can be easily retrieved:

$$\sigma^D \rho_{\text{eff}} = \frac{3\pi^2}{64} \frac{F_1/F_0}{c_1 - c_2 F_1/F_0}, \quad (4.97)$$

where the coefficients c_1 and c_2 are equal to:

$$\begin{aligned} c_1 &= (z+H)(\gamma_1 - \gamma_0), \\ c_2 &= (z+H)\gamma_0 - R/3. \end{aligned} \quad (4.98)$$

Within the approximation of Fraunhofer diffraction, the scattering cross-section equals the cross-sectional area of a scattering particle. Therefore, the scattering coefficient is:

$$\sigma^D = \langle \pi r^2 \rangle C_N = \langle \pi r^2 \rangle \frac{C_V}{\langle 4\pi r^3/3 \rangle} = \frac{3}{4} \frac{C_V}{r_{32}}, \quad (4.99)$$

where C_N is the numeric particle concentration and C_V is the volume particle concentration.

It should be noted that the diffraction scattering coefficient σ^D used here is approximately twice less than the total Mie scattering coefficient.

For the product of σ^D by ρ_{eff} , we get:

$$\sigma^D \rho_{\text{eff}} = \frac{3}{4} \frac{C_V}{r_{32}} \frac{2\pi r_{32}}{\lambda_{\text{eff}}} = \frac{3\pi}{2} \frac{C_V}{\lambda_{\text{eff}}}. \quad (4.100)$$

This means that through the ratio F_1/F_0 one can retrieve the volume concentration of droplets using the following simple formula:

$$C_V = \lambda_{\text{eff}} \frac{\pi}{32} \frac{F_1/F_0}{c_1 - c_2 F_1/F_0}. \quad (4.101)$$

Table 4.1 represents an example of such a retrieval. The five types of clouds with the droplets distribution (4.80) and different effective sizes were used for modelling. The scattering coefficient for all the cloud types was taken of 0.01 m^{-1} , the sounding depth is 100 m. The retrieved and true volume concentrations (and the relative error of retrieval, as well) are shown in Table 4.1. As can be seen, the retrieval error is not greater than 20%, but it increases with sounding depth, when the double-scattering approximation becomes invalid. The applicability of the formula (4.101) is bounded by small optical depths (about unity), as well as by the conditions (4.86) and (4.92) imposed on the geometry of an experiment. However, the use of formula (4.101) requires no additional knowledge about the properties of the medium and it can be used as a reference point in other algorithms.

Table 4.1. Example of the droplets volume concentration retrieval from Eq. (4.97)

Effective radius (μm)	True concentration (ppm)	Retrieved concentration (ppm)	Relative error (%)
4	0.02462	0.02924	18.7
6	0.03764	0.04177	11.0
8	0.05072	0.05324	5.0
10	0.06383	0.06350	-0.5
12	0.07698	0.07256	-5.7

4.5.3 The algorithm of simultaneous retrieval of the scattering coefficient and the effective droplet size

Within the single scattering approximation, the scattering coefficient can be found through the logarithmic derivative:

$$\varepsilon^0(z) = -\frac{1}{2} \frac{d}{dz} \ln \left[F_R(z) (z + H)^2 \right], \quad (4.102)$$

However, if the single scattering albedo and the phase function are known, the scattering coefficient can also be found in the case of significant influence of

multiple scattering. It can be done within the following iterative scheme: the starting scattering profile is found through Eq. (4.102), then the contribution of multiple scattering is found and the scattering profile is corrected with regard to multiple scattering. The formula for this iterative scheme is:

$$\varepsilon^{k+1}(z) = \varepsilon^k(z) - \frac{1}{2} \frac{d}{dz} \ln \left[\frac{F_R(z)}{F_R(\varepsilon^k(z))} \right], \quad (4.103)$$

where $F_R(z)$ denotes the measured signal and $F_R(\varepsilon^k(z))$ denotes the signal, calculated with account for multiple scattering with the extinction profile $\varepsilon^k(z)$ (the extinction coefficient is equal to the scattering coefficient for clouds in the visible range).

Therefore, Raman lidar sounding of warm clouds with an MFOV receiver makes possible the simultaneous retrieval of both the extinction coefficient profile and the effective size of droplets.

Let us consider the abovementioned measurement scheme. As was shown, if the scattering profile is known (the single scattering albedo for clouds is equal to unity in the visible), one can easily retrieve the effective radius of droplets through the ratio of two signals, the first being determined mainly by single scattering (F_0) and the second being determined exclusively by multiple scattering (F_1). This means that the extinction profile retrieval should be the first step. It can be done within the single scattering approximation, using the signal F_0 :

$$\varepsilon^0(z) = -\frac{1}{2} \frac{d}{dz} \ln \left[F_0(z) (z + H)^2 \right]. \quad (4.104)$$

Then, using the ratio F_1/F_0 , the effective radius of droplets is retrieved. If the retrieval accuracy is insufficient, knowing the particles size (i.e., the phase function), one can correct the extinction profile with regard to multiple scattering:

$$\varepsilon^{k+1}(z) = \varepsilon^k(z) - \frac{1}{2} \frac{d}{dz} \ln \left[\frac{F_0(z)}{F_0(\varepsilon^k(z), r_{32}^k)} \right], \quad (4.105)$$

where $\varepsilon^k(z)$ denotes the k th iteration of the extinction profile, r_{32}^k is the k th iteration of the effective radius, $F_0(z)$ is the ‘true’ signal, measured with FOV γ_0 , and $F_0(\varepsilon^k(z), r_{32}^k)$ is the signal, simulated with the profile $\varepsilon^k(z)$ and the effective radius r_{32}^k .

New value of r_{32}^{k+1} is found through the ratio F_1/F_0 with new profile $\varepsilon^{k+1}(z)$. The iterations go on until the required accuracy is achieved.

The example of such retrieval is presented in Fig. 4.5 and in Table 4.2. Only 0th (starting) and 11th iterations are plotted in Fig. 4.5. The first six iterations are shown in Table 4.2. It is seen that the retrieval within the single scattering approximation can underestimate the value of the extinction coefficient by two times, whereas after ten iterations the retrieved profile in fact replicates the true one. The derived value of r_{32} is fairly accurate at the first iteration (overestimated of about 10%) and converges rapidly to the true value.

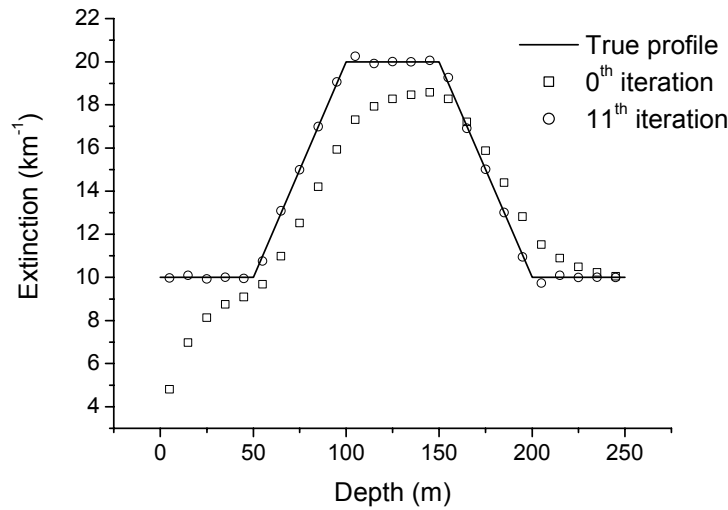


Fig. 4.5. Example of the extinction profile retrieval.

Table 4.2. Example of the effective droplets radius retrieval

Iteration number	1	2	3	4	5	6
Effective radius (μm)	6.57	5.84	6.02	6.02	6.01	6.00

4.6 Conclusion

This chapter has given a review of the main methods of Raman lidar sounding. It has displayed the advantages of and the additional possibilities in the remote sensing of the environment due to the usage of Raman lidars. It was emphasized that most of the methods of processing Raman lidar data rely on the lidar equation formulated within the single scattering approximation. The analytical theory of the Raman lidar return with regard to multiple scattering has been described in this chapter in great depth. The theory is based on the developed earlier approach of small-angle quasi-single scattering approximation, used to describe multiple scattering in usual (elastic) lidar sounding. The investigation of the angular structure of the Raman lidar return made it possible to relate the angular characteristics of multiple scattering to the microphysical characteristics of a sounding medium and to suggest the method of their retrieval by measuring the Raman lidar return with a multiple-field-of-view receiver, parting multiple scattering. In particular, the method of measuring the extinction coefficient and also the effective radius of droplets in warm clouds was described. The method could have an advantage over the similar method when using elastic scattering, because of the simple angular behaviour of the Raman backscattering phase function.

Acknowledgment

The author is grateful to Eleonora P. Zege for her support at all stages of the work and to Vera Lozanova for her help in preparing this chapter.

References

- Ansmann, A., M. Reibesell, and C. Weitkamp, 1990: Measurement of atmospheric aerosol extinction profiles with Raman lidar, *Opt. Lett.*, **15**, 746–748.
- Ansmann, A., M. Riebesell, U. Wandinger, C. Weitkamp, E. Voss, W. Lahmann, and W. Michaelis, 1992a: Combined Raman elastic-backscatter lidar for vertical profiling of moisture, aerosol extinction, backscatter, and lidar ratio, *Appl. Phys. B*, **55**, 18–28.
- Ansmann, A., U. Wandinger, M. Riebesell, and C. Weitkamp, 1992b: Independent measurement of extinction and backscatter profiles in cirrus clouds by using a combined Raman elastic-backscatter lidar, *Appl. Opt.*, **31**, 7113–7131.
- Bissonnette, L., and D. Hutt, 1990: Multiple scattering lidar, *Appl. Opt.*, **29**, 5045–5046.
- Bruscaglioni, P., M. Gai, and A. Ismaelli, 1999: Molecular lidar and Mie multiple scattering, MUSCLE 10 (International Workshop on Multiple Scattering Lidar Experiments): Proceedings, Florence, Italy, 19–22 April 1999, 206–211.
- Cohen, A., M. Kleiman, and J. Cooney, 1978: Lidar measurements of rotational Raman and double scattering, *Appl. Opt.*, **17**, 1905–1910.
- Cooney, J., 1972: Measurements of atmospheric temperature profiles by Raman backscatter, *Appl. Meteorol.*, **11**, 108–112.
- Deirmendjian, D., 1969: *Electromagnetic Scattering on Spherical Polydispersions*, Elsevier, New York.
- Egert, S., A. Cohen, M. Kleiman, and N. Ben-Yosef, 1983: Instantaneous integrated Raman scattering, *Appl. Opt.*, **22**, 1592–1597.
- Eloranta, E., 1972: Calculation of doubly scattered lidar returns, Ph.D. dissertation, University of Wisconsin, Madison.
- Fiocco, L., Z. Smullin, 1963: Detection of scattering layers in the upper atmosphere (60–140 km) by optical radar, *Nature*, **199**, 1275–1276.
- Girolamo, P. D., A. Behrendt, and V. Wulfmeyer, 2006: Spaceborne profiling of atmospheric temperature and particle extinction with pure rotational Raman lidar and of relative humidity in combination with differential absorption lidar : performance simulations, *Appl. Opt.*, **45**, 2474–2494.
- Grund C., and E. Eloranta, 1991: University of Wisconsin high spectral resolution lidar, *Opt. Eng.*, **30**, 6–12.
- Katsev, I. , E. Zege, A. Prikhach, and I. Polonsky, 1997: Efficient technique to determine backscattered light power for various atmospheric and oceanic sounding and imaging systems, *JOSA A*, **14**, 1338–1346.
- Klyshko, D. N., and V. V. Fadeev, 1978: Remote detecting the water impurity by means of laser spectroscopy calibrated by Raman scattering, *Reports of Academy of Sciences of the USSR*, **238**, 320–323 (in Russian).
- Kokhanovsky, A. A., and E. P. Zege, 1997: Parametrization of local optical characteristics of cloudy media, *Izv. Atmos. and Ocean. Phys.*, **33**, 190–198.

- Lee, Z. P., K. L. Carder, S. K. Hawes, R. G. Steward, T. G. Peacock, and C. O. Davis, 1994: Model for the interpretation of hyperspectral remote-sensing reflectance, *Appl. Opt.*, **33**, 5721–5732.
- Malinka, A., and E. Zege, 2001: Analytical modeling of the Raman lidar return including multiple scattering, *Current Problems in Optics of Natural Waters (ONW-2001)*: Proceedings of International Conference, St. Petersburg, 25–29 September 2001, 176–181.
- Malinka, A., and E. Zege, 2003a: Analytical modeling of the Raman lidar return from clouds and ocean including multiple scattering, *MUSCLE-12, Proc. of SPIE*, **5059**, 153–159.
- Malinka, A., and E. Zege, 2003b: Analytical modeling of the Raman lidar return, including multiple scattering, *Appl. Opt.*, **24**, 1075–1081.
- Malinka, A., and E. Zege, 2003c: Using multiple scattering in Raman lidar sounding of warm clouds, *6th International Symposium on Tropospheric Profiling: Needs and Technologies (ISTP-2003)*: Proceedings, Leipzig, Saxony, Germany, 14–20 September 2003, 297–299.
- Mattis, I., A. Ansmann, D. Althausen, V. Jaenisch, U. Wandinger, D. Mueller, Y. Arshinov, S. Bobrovnikov, and I. Serikov, 2002: Relative-humidity profiling in the troposphere with a Raman lidar, *Appl. Opt.*, **41**, 6451–6462.
- McLean J. W., J. D. Freeman, and R.E. Walker, 1998: Beam Spread Function with Time Dispersion, *Appl. Opt.*, **37**, 4701–4711.
- Mobley, C., B. Gentili, H. Gordon, Z. Sin, G. Kattautar, H. Morel, P. Reinersman, K. Stamnes, and R. Stavn, 1993: Comparison of numerical models for computing underwater light fields, *Appl. Opt.*, **32**, 7484–7503.
- Mueller, D., U. Wandinger, and A. Ansmann, 1999a: Microphysical particle parameters from extinction and backscatter lidar data by inversion with regularization: theory, *Appl. Opt.*, **38**, 2346–2357.
- Mueller, D., U. Wandinger, and A. Ansmann, 1999b: Microphysical particle parameters from extinction and backscatter lidar data by inversion with regularization: simulation, *Appl. Opt.*, **38**, 2358–2367.
- Mueller, D., U. Wandinger, and A. Ansmann, 2000: Microphysical particle parameters from extinction and backscatter lidar data by inversion with regularization: experiment, *Appl. Opt.*, **39**, 1879–1892.
- Muscari, G., M. Cacciani, G. Giuliani, and G. Fiocco, 1996: An imaging lidar for multiple scattering measurements, *Advances in Atmospheric Remote Sensing with Lidar: selected papers of the 18th International Laser Radar Conference (ILRC)*, Berlin, 22–26 July 1996, Springer, Berlin, 103–106.
- Piironen, P., E. Eloranta, 1994: Demonstration of a high-spectral-resolution lidar based on an iodine absorption filter, *Opt. Lett.*, **19**, 234–236.
- Polonsky, I. N., E. P. Zege, I. L. Katsev, 2001: Lidar sounding of warm clouds and determination of their microstructure parameters, *Izv. Atmos. and Ocean Phys.*, **37**, 624–632.
- Reichardt, J., M. Hess, A. Macke, 2000: Lidar inelastic multiple-scattering parameters of cirrus particle ensembles determined with geometrical-optics crystal phase functions, *Appl. Opt.*, **39**, 1895–1910.
- Reichardt, J., U. Wandinger, M. Serwazi, and C. Weitkamp, 1996: Combined Raman lidar for aerosol, ozone, and moisture measurements, *Opt. Eng.*, **5**, 1457–1465.
- Roy, G., L. Bissonnette, C. Bastille, and G. Vallee, 1997: Estimation of cloud droplet-size density distribution from multiple-field-of-view lidar returns, *Opt. Eng.*, **36**, 3404–3415.

- Samokhvalov, I.V., 1979: Double scattering approximation of the lidar equation for inhomogeneous atmosphere, *Opt. Lett.*, **4**, 12–14.
- Sherlock, V., A. Hauchecorne, and J. Lenoble, 1999a: Methodology for the independent calibration of Raman backscatter water-vapour lidar system, *Appl. Opt.*, **38**, 5816–5837.
- Sherlock, V., A. Garnier, A. Hauchecorne, and P. Keckhut, 1999b: Implementation and validation of a Raman lidar measurement of middle and upper tropospheric water vapour, *Appl. Opt.*, **38**, 5838–5850.
- Shiple, S. et al., 1983: High spectral resolution lidar to measure optical scattering properties of atmospheric aerosols. 1. Theory and instrumentation, *Appl. Opt.*, **22**, 3716–3724.
- Tomasi, F., M. R. Perrone, and M. L. Protopapa, 2001: Monitoring O₃ with Solar-Blind Raman Lidars, *Appl. Opt.*, **40**, 1314–1320.
- van de Hulst, H. C., 1957: *Light Scattering by Small Particles*, Chapman & Hall, London.
- Wandinger, U., 1998: Multiple-scattering influence on extinction and backscatter-coefficient measurement with Raman and high-spectral-resolution lidars, *Appl. Opt.*, **37**, 417–427.
- Wandinger, U., A. Ansmann, J. Reichardt, and T. Deshler, 1995: Determination of stratospheric-aerosol microphysical properties from independent extinction and backscattering measurements with Raman lidar, *Appl. Opt.*, **34**, 8315–8329.
- Weinman, J., and S. Shipley, 1972: Effects of multiple scattering on laser pulses transmitted through clouds, *J. of Geophys. Res.*, **77**, 7123–7128.
- Whiteman, D., and S. Melfi, 1999: Cloud liquid water, mean droplet radius, and number density measurements using a Raman lidar, *J. Geophys. Res. D*, **134**, 31411–31419.
- Zege, E., A. Ivanov, and I. Katsev, 1991: *Image Transfer Through a Scattering Medium*, Springer-Verlag, Berlin, Heidelberg.
- Zege, E., I. Katsev, and I. Polonsky, 1995: Analytical solution to LIDAR return signals from clouds with regards to multiple scattering, *Appl. Phys. B*, **60**, 345–354.
- Zege, E. et al., 2003a: Analytical and computer modeling of the ocean lidar performance, *MUSCLE-12, Proc. of SPIE*, **5059**, 189–199.
- Zege E., I. Katsev, A. Prikhach, and G. Ludbrook, 2001: Computer simulation with regard to pulse stretching for oceanic lidar return, *ONW-2001 (Current Problems in Optics of Natural Waters)*: Proceedings of the International Conference, St. Petersburg, Russia, 25–29 September 2001, 255–262.